Scientia Iranica, Vol. 14, No. 5, pp 474 485

SCIENTIA IRANICA

Design of a Zone Refiner for Optimization Studies

J. Haas[1], Y.C. Liu[1] and S. Dost*

Many of the physical properties of semiconductor materials depend on the presence of imperfections. A significant source of lattice imperfections is the inclusion of foreign atoms, or impurities. Since most semiconductor devices require accurate and repeatable results, highly pure materials are desired. In order to obtain high purity semiconductor metals, zone purification is commonly utilized as the final purification stage. The University of Victoria Crystal Growth Lab (CGL) Group is carrying out an optimization study of the zone refining process. To provide the required experimental platform for this study, a zone refining test bench ("CGL zone refiner") was developed. The apparatus will be used to study the effects of zone geometry and mixing on the efficiency of the zone refining process. It also has the capability of zone refining, under an applied rotating magnetic field and an electric current, in order to examine their effect. A series of preliminary experiments were carried out with the CGL zone refiner prior to optimization testing. Samples were removed from the processed ingots and sent for glow discharge mass spectrometry (GDMS) analysis. The GDMS results indicated that the system operates efficiently and that, even with as few as three zone passes, the CGL zone refiner purified the material. A numerical thermal analysis for the zone refining of Te is also presented. In general, the numerical results were in agreement with experimental observations; the solid/liquid interface was convex (toward liquid) for small liquid zones, concave for large liquid zones and the system was thermally stable.

INTRODUCTION

The production and industrial applications of semiconductors have developed dramatically since initial research with devices in the early 1950's. Today, semiconductors are used in various applications, such as solar cells, power devices, imaging detectors and more [1]. Semiconductor materials can be utilized in their pure single crystal form, but are also commonly doped or compounded with other materials to obtain the specific optical and electric properties desired for a device.

Many of the properties of crystals depend on the presence of imperfections [2]. A significant source of lattice imperfection is in the inclusion of foreign atoms, or impurities and even trace levels of impurities are known to have significant harmful effects on the performance of imaging devices [3,4]. Since most semiconductor devices require highly accurate and repeatable results, extremely pure materials are required, in order to obtain predictable and consistent properties.

Semiconductor materials are most commonly extracted from primary ores; these are then purified through various chemical, electrolytic and pyrometallurgical methods [1,5]. The electrochemical procedures are utilized for the gross initial purification steps and yet relatively high levels of impurities remain. Zone refining is commonly used as the last step in the purification process and is an important final procedure in the purification of materials. Currently, materials are being commercially produced with purities up to and exceeding 7N (99.99999%), using zone refining.

Although there are indications that work was being carried out with the process as early as the 1930's [6], zone refining was first introduced to the public in 1952 by Pfann [7]. The creation and quick advancement of rectifiers and transistors created a demand for high purity germanium after WWII and this produced a need for more effective purification methods. During this period, Pfann stumbled across the idea of zone purification [8] and has since published many articles, as well as an authoritative book, on the subject [9]. Zone refining usually takes advantage of the difference in composition between the solid

1. *Crystal Growth Laboratory, Department of Mechanical Engineering, University of Victoria, Victoria, BC, V8W 3P6, Canada.*

*. *Corresponding Author, Crystal Growth Laboratory, Department of Mechanical Engineering, University of Victoria, Victoria, BC, V8W 3P6, Canada.*

and liquid phases, but it can be used to purify any material which has a varied composition between two phases. The technique has been applied to metals and semiconductors, as well as to organic and inorganic compounds [10].

Presently, the University of Victoria Crystal Growth Lab (CGL) Group is carrying out a study of the zone refining process. The main objective of this project is the identification and demonstration of the optimum process parameters and equipment configuration that will allow for the production of larger ingots, while minimizing process time and maintaining or improving the process efficiency and overall material yield. In order to carry out the experimental portion of this project, a test-bench zone refiner, "CGL zone refiner", was designed and developed. The apparatus was built to study the effects of zone geometry and mixing on the efficiency of the process. It was also built with the capability of using an applied rotating magnetic field on the middle heater and an applied electric current through the ingot to examine the effect of magnetically induced mixing and electromigration.

This article discusses the relevant theory of zone refining, as well as the design and initial testing of the UVic CGL zone refiner. It also outlines a numerical thermal analysis carried out for the zone refining system.

ZONE PURIFICATION

Zone melting refers to the various methods of controlling the distribution of impurities, or solutes, in a crystalline solid [9]. During the zone melting process, a series of molten zones pass through a charge in one direction and impurities travel with, or opposite to, the zones, concentrating them at one end of the charge. Using the difference in composition between the freezing solid and liquid phases, zone melting permits the manipulation of impurities distributed in a material; for example, it can be used for purification (zone refining), uniformly distributing a desired impurity (zone levelling) and single crystal growth, among others. Zone refining can be used for purification of any material that can be safely melted and that exhibits a difference in impurity concentration between the liquid and solid phases [9].

The Process

When a relatively large amount of molten metal with low concentrations of impurities, or solute, is allowed to cool, the composition at the freezing interface is generally different from the melt. The composition in the freezing solid can be richer or poorer in solute; this results in a boundary layer in front of the freezing interface that has decreased or increased solute concentration (see Figure 1). From this, it can be said that the freezing interface either attracts or rejects impurities. The solute-rich (or depleted) boundary layer results in an inequilibrium of concentration in the melt and diffusion takes place. Segregation occurs as the impurities diffuse through the melt and the molten zone traverses along the ingot; the distribution of these impurities depends on the distribution coefficient, k.

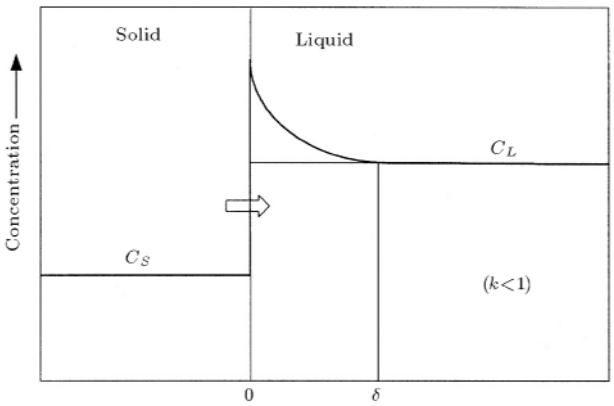

Figure 1. Solute concentration profile for an advancing solid-liquid interface.

The distribution coefficient can either be greater or less than unity, depending on whether the solute raises or lowers the melting point of the base material, or solvent. The equilibrium distribution coefficient, k_0, can be taken from the phase diagram, as shown in Figure 2 and is defined as the ratio of the solute concentration in the freezing solid to that in the main body of the liquid [9]:

$$k_0 = \frac{C_S}{C_L}. \tag{1}$$

But the theoretically predicted equilibrium distribution coefficient is not usually observed under normal conditions [3]. The term, effective distribution coefficient, k_{eff}, is used to describe the segregation of an impurity as observed in practice and is defined as the ratio of the solute concentration in the freezing solid to that in the enriched liquid boundary layer, $C_L^*(k_{eff} = C_S/C_L^*)$. This can be calculated by:

$$k_{\text{eff}} = \frac{1}{1 + (1/k_0 \quad 1)e^{\ f\delta/D)}}, \tag{2}$$

where f represents growth rate (zone speed), D is the diffusivity in the liquid, δ stands for the boundary layer thickness and $f\delta/D$ is known as the normalized growth velocity [9].

Zone refining is usually divided into three cases for examination: After one pass, after successive passes, and after an indefinitely large number of passes. The ultimate distribution is achieved in this last case and results in the maximum purification possible for a given ingot [9].

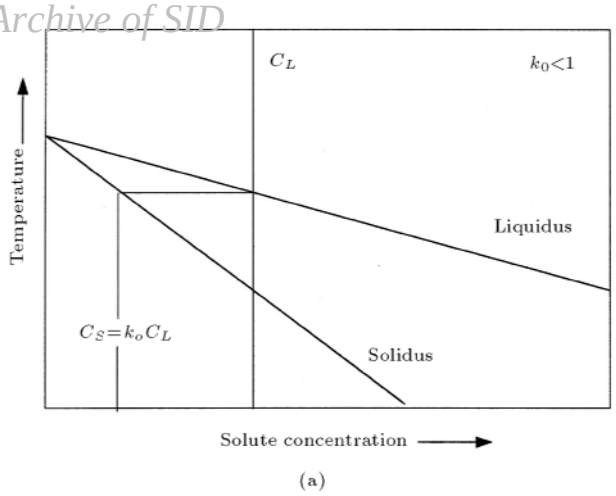

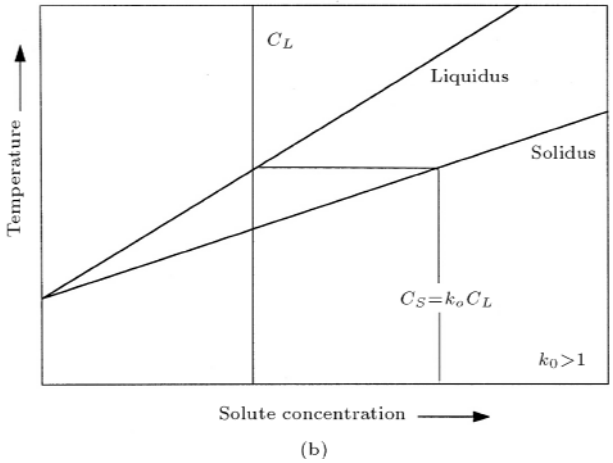

Figure 2. Portion of phase diagram in which the freezing point of the solvent is a) lowered, b) raised by the solute or impurity.

The advantages of zone refining are only seen when multiple passes are used; single pass zone refining results in less purification than simple normal freezing [9]. By using a series of closely spaced heaters, any desired number of molten zones can be traversed through the ingot in a single operation, allowing for increased purification. Once processed, the initial ingot region will contain higher concentrations of solute that raise the melting temperature of the material ($k_{\text{eff}} > 1$); the end region will contain higher concentrations of solute that lower the melting temperature of the material ($k_{\text{eff}} < 1$); and the middle region will be depleted of all solute, with $k_{\text{eff}} \neq 1$.

After numerous zone passes, the concentration distribution reaches a steady-state, or ultimate distribution. At this point, the amount of solute solidifying out at the freezing interface is equal to that which is added at the melting interface. An approximation to the ultimate distribution is given by the equation [9]:

$$C(x) = Ae^{Bx}, \tag{3}$$

where the constants, A and B, can be obtained from:

$$k_{\text{eff}} = \frac{Bl}{e^{Bl} \quad 1},$$

and:

$$A = \frac{C_0 BL}{e^{BL} \quad 1}, \tag{4}$$

where C_0 is the initial impurity concentration, l is the molten zone length and L is the length of the ingot. An example of ultimate distributions for varied k_{eff} values is shown in Figure 3.

Optimization

With any given material being zone refined, it is possible to achieve higher purity simply by passing additional molten zones through the ingot (up to the ultimate distribution). Nevertheless, each additional run requires time and increases production costs. In an attempt to increase efficiency, efforts have been made to quantify and optimize the process and equipment, in order to reduce production time and costs. Some of the optimization techniques are based on manipulating the effective distribution coefficient or varying zone lengths.

The simplest way to increase the efficiency of zone refining is to manipulate the process variables that influence the effective distribution coefficient. It can be seen from the equation for the effective distribution coefficient, given in Equation 2, that the zone rate and boundary layer thickness affect k_{eff}. This is illustrated in the plot of distribution coefficient vs. boundary layer thickness for varied zone speeds, given in Figure 4.

As seen in Figure 4, k_{eff} approaches unity faster, as zone speed and boundary layer thickness increase, resulting in reduced segregation. In order to optimize the process, k_{eff} must be brought as close to k_0 as

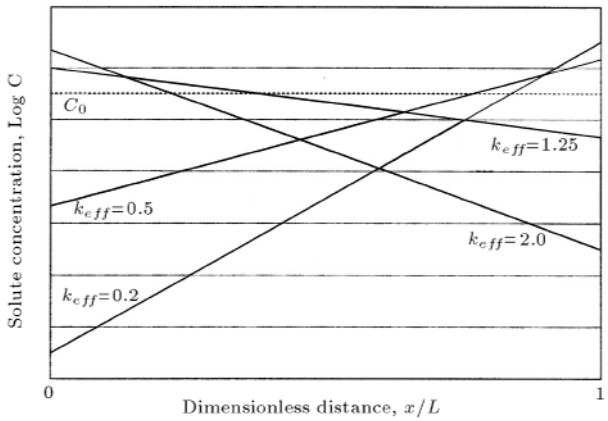

Figure 3. Ultimate distribution curves for various k values.

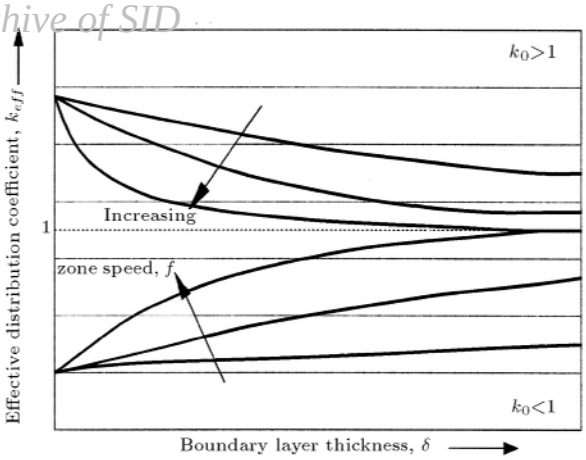

Figure 4. The effect of zone speed and boundary layer on k_{eff}.

possible by reducing the boundary layer thickness and zone travel rate.

While lower zone speeds increase the segregation efficiency (up to the extreme, approaching equilibrium freezing), they result in longer process times or fewer passes per unit time. The time required to achieve a specific purity level varies directly with the number of passes (n) and, inversely, with the zone speed (f); the ratio, n/f, for a given k_{eff}, provides a direct measure of this time [9]. When several impurities are involved, the optimal travel rate is determined by the one whose k_{eff} is closest to unity [9].

Minimizing the boundary layer thickness also increases the segregation of impurities. The boundary layer thickness is directly influenced by the degree of mixing or diffusion in the melt. Mixing can be achieved through mechanical stirring, or increased transport within the molten zone through applied magnetic and/or electric fields. A trade off between the variables, while keeping $f\delta/D$ approximately constant, can also decrease production time, e.g., increased mixing allows for higher zone rates.

Convection within the molten zone can also be enhanced by a higher temperature gradient, due to increased heat input [11], but, it has also been shown that the temperature of the molten zone can affect the effective distribution coefficient for some impurities. In general, higher molten zone temperatures reduce the segregation efficiency [12].

More effective, but more complicated, methods of optimization have also been developed using varied zone lengths [11,13,14]. There have been several different methods in which the optimum zone length has been analyzed. In all of the models presented, assumptions were made to simplify calculations, such as constant density upon melting, constant distribution coefficient and complete mixing of the molten zone.

In all of these simulations, there is agreement in some of the fundamental effects of the zone length on segregation. The most significant characteristic of the zone length presented is that longer zones are more efficient for early passes, and shorter zones for later passes [9,11,13-17]. Long zones favour more rapid initial purification, because, as the interface moves, rejected impurity is diluted into a larger volume of material [13]. It has been shown numerous times that the optimal zone length for the first pass is the entire ingot (normal freezing) for all values of k_{eff} [9,11,13-17]. The length of the molten zone also affects both the ultimate distribution and the rate at which it is approached. Short zones allow much better ultimate distributions to be achieved [11].

It is also generally agreed upon that the optimal zone length increases with the distribution coefficient, but, decreases with pass number [14,15]. This holds true, except for continuously varied zone lengths, where it has been shown that there is no dependence on the distribution coefficient [13,14].

ZONE REFINER DEVELOPMENT

The CGL apparatus, shown in Figure 5, was designed as a three zone, multi-pass zone refiner, with fixed heaters and a translating charge. The zone refiner has the capability to adjust all of the process variables which will allow it to examine any combination of variables, required for optimization studies.

Translation of molten zones through the ingot was achieved using a programmable linear system. An example of the heater movements required for translating molten zones using multiple heaters is given in Figure 6 (in the figure, the two heaters are translated and the tube static to better show the relative movement; on the CGL zone refiner the heaters are fixed and the tube translated). First, the tube is slowly translated at the desired rate, the distance of one heater spacing. (See Figures 6a to c.) Once the tube reaches the end of this movement, it is returned quickly back to the start

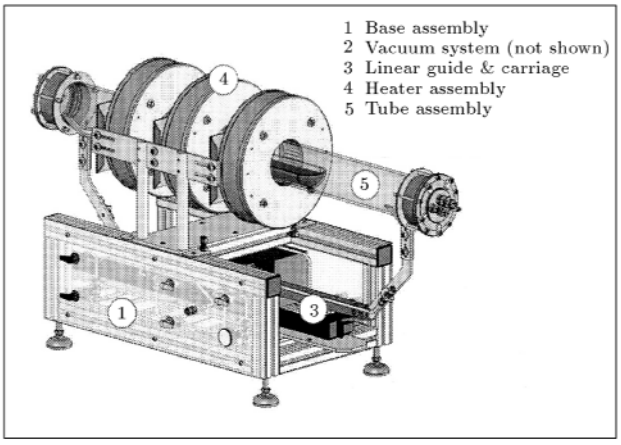

Figure 5. CGL zone refiner CAD model.

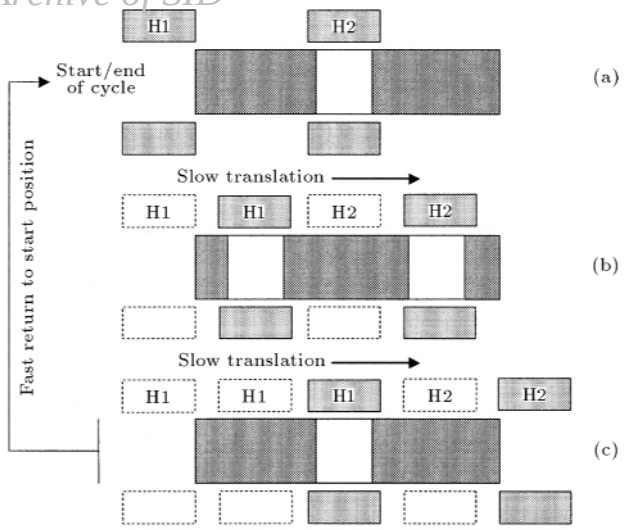

Figure 6. Heater cycle and molten zone movement diagram for passing multiple zones with two heaters (H1 and H2).

position (Figures 6c to a). The molten zone left by one heater (H1) is recaptured by the heater in front of it (H2). Slow translation is then started again. This translation-return reciprocating heater cycle can be repeated for as many molten zone passes as desired.

Once the design and assembly of the CGL zone refiner system was completed, a series of tests were carried out to prove and characterize the system. First, the zone refiner was charged with tellurium and thermal testing carried out, in order to determine the characteristics of the apparatus. Then, once confidence in the system's operation had been attained, full process tests could be initiated. A series of three-zone pass tests were performed and samples removed from the purified ingots.

Samples were removed from the tip and tail of each ingot, as well as equally along the length in between. Samples were removed from as near to the center of the ingot as possible; the exact position was affected by the material grain structure as it was much more difficult to break across the grain and often hard to extract a sample from an exact position. Three samples each from the third and eighth experiments were sent for glow discharge mass spectrometry (GDMS) analysis by the Chemical Metrology Group at the National Research Council of Canada Institute for National Measurement Standards. Financial considerations prevented GDMS analysis of all of the samples from each experiment.

All handling of the charge material was carried out in the CGL cleanroom with material-specific containers and tools to avoid contamination. The charge material was kept in a clean environment at all times while inside the zone refiner, even when an experiment was not in progress.

EXPERIMENTAL RESULTS

Table 1 presents the GDMS data indicating the residual impurities in the samples tested from the third and eighth three-zone pass experiments. GDMS results from the source material are included for comparison. Both a partial and full analysis were carried out on the source material, which gave results that illustrated the accuracy of the GDMS analysis.

The "less than" in Table 1 indicates the maximum concentration level. It is probable that the actual concentration is lower, but it is impossible to distinguish the specific element given the GDMS output. This is due to the reduced visibility of the individual mass readings correlating to the target element, either from noise, due to interaction with the surrounding physical environment, or elemental compounds. At such low concentrations, it is difficult to determine the exact level of impurities, given the GDMS accuracy. A consequence of this is the inability to make definite conclusions on the purification efficiency, with respect to many of the impurities.

The objective of analyzing samples from the two ingots was to determine if the apparatus was operating as desired, that is, if purification of the material occurred and if any impurities were introduced during the process. If an impurity were introduced during handling or zone refining, a significant increase in the impurity concentration would be seen after running multiple experiments. However, in general, a reduction in concentration was observed for all impurities tested with no unexpected spikes in concentration. Because of this, it can be concluded that there were no external sources of contamination from the CGL process.

The GDMS data in Table 1 also shows that the CGL zone refiner is capable of purifying an ingot of tellurium. Even with as few as three full zone passes, there was some removal of many of the impurities. There were exceptionally low concentrations of carbon, nitrogen and oxygen in the purified ingot from the third test, compared to the source material. These values, obtained with the CGL zone refiner, were even significantly lower than those attainable using the commercial apparatus. It is unclear exactly why the CGL zone refiner was considerably more efficient at removing the C, N and O during this experiment. The residual concentrations of C, N and O in the ingot from the eighth test were at a level more representative of the commercial apparatus's capability.

Most of the impurities in the ingots appeared in very low residual concentrations; the readings were too low to distinguish any concentration profile along the ingot. However, the level of a few impurities remained high enough to produce a concentration profile. Some elements from the third test, such as silicon (see Figure 7a), showed a concentration profile

Table 1. GDMS data.

Institute for National Measurement Standards Chemical Metrology			Glow Discharge Mass Spectrometric Report ppb (Atomic)					
	Te Source		Test #3 Samples			Test #8 Samples		
Element	Partial	Full	Tip	Middle	Tail	Tip	Middle	Tail
Li		<6	<9	<8	<9	<8	<7	<12
Be	<14	<5	<7	<7	<8	<7	<6	<8
B	<7	<6	<7	<7	<5	<6	<5	<9
C		950	29	36	43	450	290	700
N		280	4	4	5	55	45	80
O		1300	57	56	20	980	580	1000
F		<25	<20	<15	<10	<20	<15	<50
Na	83	<4	<5	<5	<5	<4	<4	<7
Mg	<7	<3	<4	<4	<3	<3	<3	<5
Al	26	<2	<2	<2	<2	<2	<2	12
Si	30	25	<3	8	21	<5	<7	15
P		<3	<4	<4	<3	<3	<3	<5
S	<20	<7	<4	<4	<4	<6	<5	<6
Cl		<7	<3	<3	<2	<5	<6	<8
K		<30	<10	<10	<8	<15	<15	<20
Ca	<95	<35	<30	<25	<20	<65	<45	<80
Sc		<0.9	<1	<1	<1	<2	<1	<2
Ti	9	<0.5	<0.7	<0.6	<0.4	<0.5	<0.5	<0.9
V	<0.8	<0.3	<0.5	<0.4	<0.5	<0.4	<0.4	<0.5
Cr	<3	<2	<2	<1	<2	<3	<2	<2
Mn	<2	<0.9	<1	<1	<1	<1	<1	<1
Fe	<5	<0.8	<0.7	3	<0.7	<0.7	<1	<1
Co		<0.5	<0.7	<0.7	<0.8	<0.7	<0.6	<0.7
Ni	<3	<1	<2	<2	<2	<2	<2	<2
Cu	<7	<3	<4	<5	12	<4	<3	<4
Zn	<18	<8	<11	<10	<11	<10	<9	<12
Ga	<7	<3	<4	<4	<4	<4	<3	<4
Ge	<14	<6	<8	<6	<9	<8	<7	<9
As	<4	<2	<2	<2	<3	<2	<2	<3
Se	<50	<10	<10	<10	<10	<10	<10	<10
Br								
Rb		<1	<2	<2	<2	<2	<1	<2
Sr		<0.6	<0.8	<0.8	<0.9	<0.8	<0.7	<1
Y		<0.5	<0.7	<0.6	<0.7	<0.7	<0.6	<0.8
Zr	<1	<0.5	<0.7	<0.7	<0.7	<0.7	<0.6	<0.8
Nb		<0.4	<0.6	<0.6	<0.6	<0.6	<0.5	<0.7
Mo	<2	<1	<1	<1	<1	<1	<1	<2
Pb								
Ag	<8	<3	<5	<5	<5	<5	<4	<6
Cd	<20	<8	<12	<11	<12	<9	<10	<13
In	<3	<1	<2	<2	<2	<2	<1	<2
Sn	<10	<4	<6	<6	<7	<9	<8	<8
Sb	<130	<30	<60	<95	<55	<85	<100	<80
Te	Matrix	Matrix	Matrix	Matrix	Matrix	Matrix	Matrix	Matrix
I		<550	<670	<860	<630	<950	<1000	<870
Cs		<3	<9	<9	<8	<10	<8	<8
Ba		<3	<4	<4	<3	<3	<3	<3
La		<0.4	<0.3	<0.2	<0.2	<0.7	<0.2	<0.3
Ce		<3	<0.6	<0.3	<0.2	<0.7	<0.3	<0.9
Hf		<0.6	<0.8	<0.8	<0.8	<0.8	<0.7	<0.9
Ta								
W		<0.8	<1	<1	<1	<1	<0.9	<1
Pt		<3	<4	<4	<4	<4	<3	<5
Au	<65	<10	<10	<10	<10	<10	<10	<10
Hg	<17	<4	<6	<5	<6	<5	<4	<6
Ti	<4	<2	<2	<1	<2	<2	<2	<3
Pb	<1	<0.7	<0.8	<0.7	<0.8	<0.6	<0.6	<0.8
Bi	<2	<0.5	<1	<1	<1	<1	<0.8	<1
Th		<0.2	<0.2	<0.2	<0.2	<0.2	<0.2	<0.2
U		<0.2	<0.2	<0.2	<0.2	<0.2	<0.2	<0.1

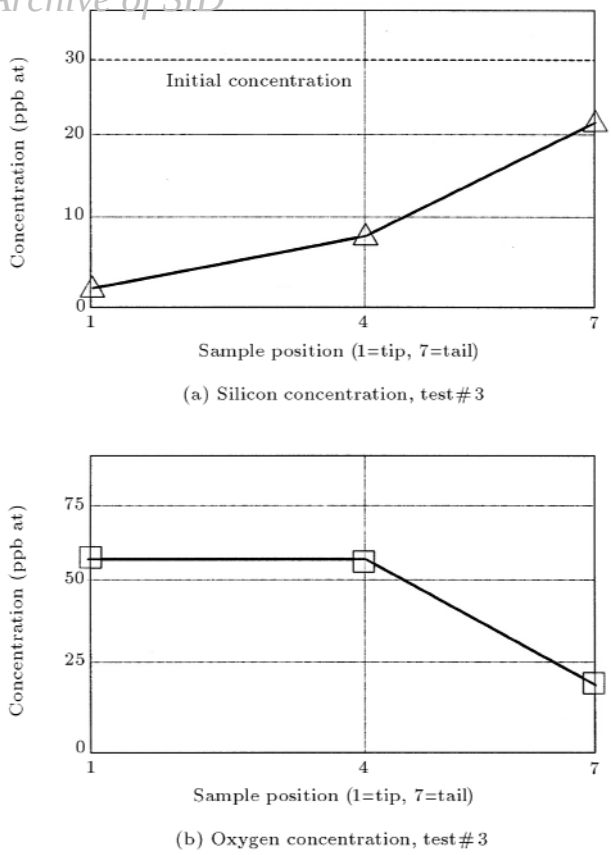

Figure 7. Residual a) Silicon and b) Oxygen concentration profiles after three- zone passes.

after the three zone passes that indicated it has an effective distribution coefficient < 1 for this system. The greatest reduction in concentration was at the tip of the ingot. Other elements, such as oxygen (See Figure 7b) (also possibly fluorine and calcium), showed a concentration profile that indicated it has an effective distribution coefficient > 1 for this system. The greatest reduction in concentration was at the tail of the ingot.

FUTURE OPTIMIZATION STUDIES

The CGL zone refiner will now be used to determine the effect on the purification efficiency using specific techniques and varying process variables. Methods will be tested that would most likely increase the efficiency (increase purity or decrease production time), based on theory and recommendations from a numerical model developed in parallel to the experimental study. The future experiments will also include the use of an applied electric current and rotating magnetic field. The reasoning for these is given briefly below.

When an electric current is passed through a molten zone, a net transport of species occurs; this transport process is referred to as electromigration or electrotransport [18]. It has been shown that the combination of electrotransport with vertical zone refining can improve the purification process [19] and also aid in crystal growth by electroepitaxy [20]. In order to examine the effect of electrotransport on purification in a horizontal system, an electric current will be applied to the CGL zone refiner. A current will be applied to the ingot across two graphite contacts, one located at each end of the ingot. A power supply connected to the graphite rods will be used to drive a current during the experiments. Impurities remaining after these experiments will be compared with the results from the standard zone refining tests to quantify the effect.

It is known that a rotating magnetic field affects mixing in the liquid phase of an electrical conducting melt [21-23]. The rotating magnetic field induces an electric field that generates an electric current, which, in turn, creates Lorenz forces. These forces drive the primary azimuthal flow in the melt (perpendicular to the rotational axis of the magnet) [21]. A significantly smaller secondary cell flow in axial and radial directions is also generated, due to pressure gradients and centrifugal forces [21]. It is anticipated that the forces generated by a rotating magnetic field around the molten zone in a horizontal zone refiner will increase mixing and, therefore, decrease the boundary layer thickness at the freezing interface. Electromagnetic coils will be placed around the center heater of the CGL zone refiner. Once installed, the effect of a rotating magnetic field on the purification efficiency will be examined.

NUMERICAL THERMAL ANALYSIS

An experimental study of the ZR process may require a large number of experiments, in order to understand the mechanisms governing the mass transport between the solid and liquid phases. Such experiments are expensive and time consuming and they must be reduced to a minimum. In addition, some aspects of the ZR process (for instance, temperature and impurity distributions) cannot be measured during the process without disturbing the process itself. However, as is the case in many other materials processing techniques, numerical simulations can provide effective and inexpensive means to shed light on many aspects of the ZR process (see, for instance [11,13-15,24-31]).

In this section, as an example, the results of a computational thermal analysis are presented, carried out for the zone refining of Te. The schematic geometry and coordinate system used in the computational domain are shown in Figure 8. The model domain consisted of (i) Three heater/insulator regions placed at equal distances along the quartz tube; (ii) The charge region, which is contained in a quartz boat within the

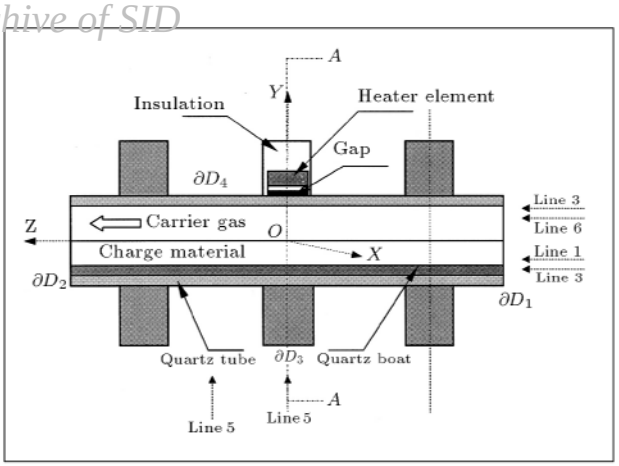

Figure 8. Schematic view of the three-zone numerical model.

quartz tube and (iii) A carrier gas region at the upper part of the quartz tube.

In the model, the gas gap between the heater and the quartz tube was ignored because of the difficulty in meshing for such a small region, which often introduced large computational errors. Instead, its influence was considered by adopting an effective thermal conductivity for the heater region. Similar treatment was given to the small gap between the quartz boat and the quartz tube. Its influence was included into the effective thermal conductivity of the quartz wall.

Computations were carried out using the commercial package "Fluent". Since translation of the quartz tube during the zone refining process is relatively slow, a pseudo-steady state was considered in the simulations. The contribution of natural convection in the molten zone to heat transfer was assumed relatively insignificant, in comparison to that of the incident radiative heat flux. Hence, only conductive heat transfer was considered within the charge [31]. Furthermore, the thermal contribution of the gas flow inside the quartz tube was neglected, due to its small flow rate and only its final state (temperature, pressure, and flow flux) at the inlet and outlet was incorporated into the energy balance of the system. Indeed, the present calculations showed that the gas flow had little influence on the overall thermal field. The solidification model provided by Fluent was employed so that changes in the zone shape could directly be seen with the thermal field. The model treated the liquid and solid phases as a single domain whose properties changed dramatically over the freezing range. Therefore, the effects of phase change and latent heat were taken into account and the interface shapes were determined by the isotherm lines. A surface-to-surface radiation model with pre-computed view factors was used to calculate the radiative heat transfer between the surfaces of the gas region, which included the heat radiation between the heater element and the charge. The model assumed a non-participating medium and optically grey and diffuse surfaces [32].

A mixed, convective and radiative boundary condition was used at the exterior surfaces of the quartz tube (∂D_4 in Figure 8) and the insulator (∂D_3):

$$q = h(T \quad T_0) + \varepsilon\sigma(T^4 \quad T_0^4), \tag{5}$$

with $T_0 = 298$ K, where h is the heat transfer coefficient, ε is the emissivity and σ is the Stefan-Boltzmann constant. At the inlet and outlet surfaces (∂D_1 and ∂D_2), a fixed mass transfer rate condition was used (at a certain temperature) for the gas region; while, for the charge region, Equation 5 was used to reflect the heat transfer.

The total mesh generated for the system was 275,184 hexahedral cells, with 5,760 cells in each of the heater regions, 54,648 in the charge and 95,040 in the gas region. The effects of thicknesses of the quartz tube and the quartz boat were considered through the corresponding boundary conditions. According to Fluent, the heat resistance at the boundary walls was approximately δ/K [32], where δ is the thickness and K the conductivity.

The physical properties of Te, quartz, insulation and the heater are presented in Table 2. The physical properties of air were used to represent the properties of the heater region. The effective conductivity (combination of heat conduction, convection and radiation at the air gap between the heater and the quartz tube) was chosen according to [33]. According to [33] and [34], the thermal conductivity of the insulation ceramics should be several times larger than its literature value of 0.13 W/m.K, due to the in-homogeneities in the insulator, such as air gaps, channels for optical sensors, thermal couples and power supply etc. Therefore, a value of 1.0 W/m.K was used in the model. The operational data is shown in Table 3. The values of heat transfer coefficient and emissivity were estimated and adjusted to better fit the zone length and shape, as well as the measured temperatures.

Results and Discussion

Figures 9a and 9b show the temperature contours at the outer surface of the quartz tube and heaters and at the Te charge region, respectively. The maximum temperature is 1134.4 K, located inside the end heater region and the minimum temperature is 354 K.

Figure 9(c) presents the temperature distribution at the surface A-A (the middle cross section along the Z-direction of the middle heater, as shown in Figure 8). There was no significant temperature difference between the charge and gas region in the quartz tube; this was due to the poor thermal conductivity of Te.

The contours of liquid fraction at the charge region are shown in Figure 9d. The numerical results

Table 2. Physical parameters.

Parameter	Value	Unit	Reference
Tellurium			
Melting point	449.5	°C	[35]
Boiling point	988.0	°C	[35]
Atomic weight	127.6		[35]
Thermal expansion coefficient	1.8×10^{-5}	K^{-1}	[35]
Latent heat of fusion	86.113	KJ/kg	[35]
Density			
Solid	6.15×10^3	kg/m^3 (at 400°C)	
Liquid	5.86×10^3	kg/m^3 (at 450°C)	
Specific Heat			[35]
Solid	227.0	J/kg.K	
Liquid	230.0	J/kg.K	
Thermal conductivity			[36]
Solid	1.8	W/m.K	
Liquid	3.8	W/m.K	
Viscosity	1.7×10^{-3}	kg/m.s	[37]
Emissivity	0.3		
Quartz			[33,38]
Density	2200.0	kg/m^3	
Specific Heat	670.0	J/kg.K	
Thermal conductivity	1.8	W/m.K (300 to 450°C)	
Emissivity	0.55		
Insulation			
Density	2300.0	kg/m^3	[39]
Specific Heat	210.0	J/kg.K	Estimated
Thermal Conductivity	1.0	W/m.K	[33,34]
Heater			
Density	1.225	kg/m^3 (air)	
Specific heat	1006.4	J/kg.K (air)	
Thermal conductivity	0.9	W/m.K	[33]

Table 3. Operational data for Te.

Heat source for the middle heater	40% of the full power
Heat source for the end heater	65% of the full power
Heat transfer coefficient (h) at the inlet and outlet of the Te charge	16 $W/m^2.K$
Emissivity at the inlet and outlet	0.2
Heat transfer coefficient (h) at the outer insulation walls	15 $W/m^2.K$
Emissivity at the insulation walls	0.2
Heat transfer coefficient (h) at the outer quartz walls	20 $W/m^2.K$
Emissivity at the outer quartz walls	0.55

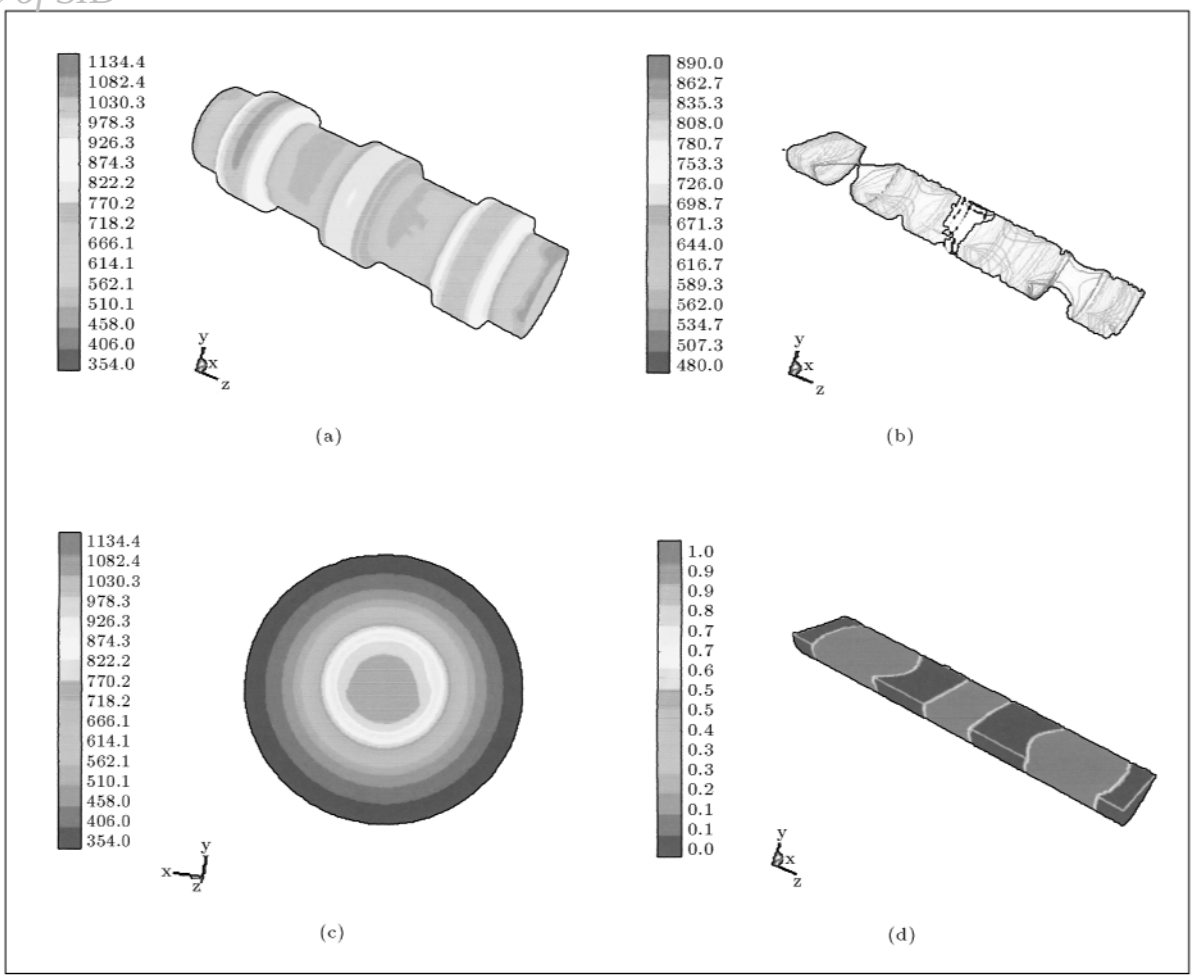

Figure 9. Simulation results for the Te-system: (a) At the exterior surfaces of quartz tube and heaters, (b) At the charge region, (c) At the surface of A-A, and (d) Contours of liquid fraction of the charge region.

generally agreed with experimental observations, but, the computed molten zone shapes were not as unsymmetric as observed in production. This can possibly be attributed to the omission of heat translation and natural convection in the molten zones in the present analysis.

Figure 10 presents the temperature distributions along lines 1 to 5, as shown in Figure 8. In the middle heater region, the highest temperature was about 777 K for Line 1 and 730 K for Line 2, while the lowest temperature, between the end and middle heater, was about 585 K for Line 1 and 653 K for Line 2 (Figure 10a). The temperature difference between the melt and solid portions along the bottom of the Te charge (Line 1) was 192 K at the middle heater region and 335 K in the end heater regions. The temperature difference at different depths of the charge (along the Y-direction) was large because of the poor conductivity of Te, indicating much stronger convection in the melt.

Figure 10b shows that, in the gas region, the maximum temperature at the end heaters was much higher than that at the middle heater, indicating a strong radiation effect at high temperatures. A similar situation can be seen in the charge region from Figure 10a. From Figure 10c, one can clearly see that the temperature at different depths of the charge differ significantly. For a certain cross section, the values and distribution of the temperature at the gas region were somewhat similar to those at the Te-charge region.

CONCLUSIONS

During both initial thermal testing and full three zone pass experiments, the CGL zone refiner performed as expected without difficulty. The entire process has been qualified and determined to be stable and easily controlled. The CGL system has been shown to be a clean process that does not introduce foreign contaminants. It is capable of refining tellurium, even with as few as three zone passes. Based on these preliminary results, one can conclude that the zone refiner developed is capable for use in the intended

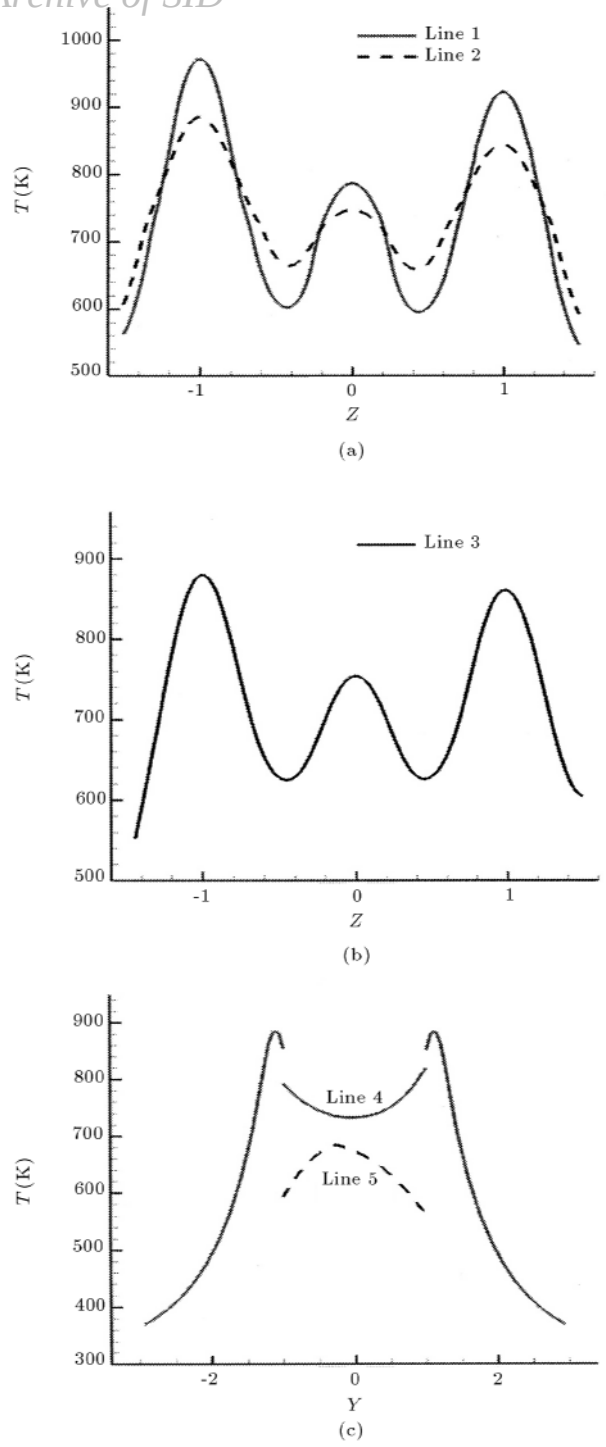

Figure 10. (a) Temperature distribution along Lines 1 and 2, (b) Temperature distribution along Line 3, and (c) Temperature distribution along Lines 4 and 5.

optimization experiments. It will now be used to determine the most efficient possible combination of system variables for this type of apparatus.

In order to determine the effect of future modifications to the apparatus on purification efficiency, lower grade material will be used for the experiments. Although the GDMS results are relatively accurate and repeatable for some impurities at low concentrations, they possess large statistical errors associated with the GDMS technique. The low levels of residual impurities obtained from the initial CGL zone refiner tests are smaller than the presented GDMS errors. The lower grade material will be used to ensure that the residual concentration of some of the impurities will remain higher than the error and no variation in concentration is a result of the GDMS readings.

The thermal analysis conducted for the zone refining of Te provided insight into the thermal properties of the system and led to the following specific conclusions. The solid/liquid interface is convex (toward liquid) for small liquid zones and concave for large liquid zones. This is in agreement with experimental observations. The Te system is stable and not sensitive to small environmental changes and the influence of the small gas gap between the quartz tube and the quartz boat on the charge region is small.

ACKNOWLEDGMENTS

The authors are grateful for the financial support from the Natural Sciences and Engineering Research Council of Canada, as well as the financial and technical support from 5N Plus Inc. of Montreal, Canada.

REFERENCES

1. Sze, S.M. *Modern Semiconductor Device Physics*, New York, Chichester, England, John Wiley (1998).
2. Kröger, F.A., *The Chemistry of Imperfect Crystals*, Amsterdam, North-Holland Pub. Co. (1973).
3. Bollong, A.B. and Roelof, P.B. "The ultrapurification of tellurium", *Journal of Metals*, **41**, pp 39-41 (1989).
4. Prasad, D.S., Sudheer, C., Munirathnam, N.R. and Prakash, T.L. "Tellurium purification: Various techniques and limitations", *Bulletin of Material Science*, **25**, pp 545-547 (2002).
5. Cooper, W.C., *Tellurium, Toronto*, Van Nostrand Reinhold Co. (1971).
6. Mackay, D.L. "Pre-history of zone-refining", *Trends in Biochemical Science*, **4**, pp N33-N33 (1979).
7. Pfann, W.G., *Trans. AIME 194*, p 747 (1952).
8. Pfann, W.G. "How zone-melting was invented", *Progress in Crystal Growth and Characterization of Materials*, **6**, pp R3-R4 (1983).
9. Pfann, W.G., *Zone Melting*, New York, Wiley (1966).
10. Pfann, W.G., Miller, C.E. and Hunt, J.D. "New zone refining techniques for chemical compounds", *The Review of Scientific Instruments*, **37**, p 649 (1966).
11. Spim, J.A.J., Bernadou, M.J. and Garcia, A. "Numerical modeling and optimization of zone refining", *Journal of Alloys and Compounds*, **298**, pp 299-305, (2000).

12. Zaiour, A. and Hamdoun, B. "Effect of temperature on segregation coefficients of impurities in tellurium", *Physica Scripta*, **70**, pp 193-196 (Aug.-Sep. 2004).

13. Rodway, G.H. and Hunt, J.D. "Optimizing zone refining", *Journal of Crystal Growth*, **97**, pp 680-688, 10 (1989).

14. Ho, C.D., Yeh, H.M. and Yeh, T.L. "The optimal variation of zone lengths in multipass zone refining processes", *Separation and Purification Technology*, **15**, pp 69-78 (1999).

15. Ho, C.D., Yeh, H.M. and Yeh, T.L. "Simulation of multipass zone-refining processes", *International Journal of Modelling and Simulation*, **23**, pp 85-93 (2003).

16. Ho, C.D., Yeh, H.M., Yeh, T.L. and Sheu, H.W. "Simulation of multipass zone-refining processes with variable distribution coefficients", *Journal of the Chinese Institute of Chemical Engineers*, **29**, pp 65-71 (1998).

17. Ho, C.D., Yeh, H.M., Yeh, T.L. and Sheu, H.W. "Simulation of multipass zone-refining processes within whole ingot", *Journal of the Chinese Institute of Chemical Engineers*, **28**, pp 271-279 (1997).

18. Jordan, R.G. "Electrotransport in solid metal systems", *Contemporary Physics*, **15**, pp 375-400 (1974).

19. King, C.A. and Brown, S.V. "The combination of electrotransport and zone-refining techniques for the growth and purification of metallic crystals", *The Review of Scientific Instruments*, **63**, pp 3185-3187 (1992).

20. Imamura, Y., Jastrzebski, L. and Gatos, H.C., *J. Electrochem*, **126**(8), pp 1381-1385 (1979).

21. Dold, P. and Benz, K.W. "Rotating magnetic fields: Fluid flow and crystal growth applications", *Progress in Crystal Growth and Characterization of Materials*, **38**, pp 7-38 (1999).

22. Volz, M.P., Walker, J.S., Schweizer, M., Cobb, S.D. and Szofran, F.R. "Bridgman growth of germanium crystals in a rotating magnetic field", *Journal of Crystal Growth*, **282**, pp 305-312 (2005).

23. Yesilyurt, S., Motakef, S., Grugel, R. and Mazuruk, K. "The effect of the traveling magnetic field (TMF) on the buoyancy-induced convection in the vertical Bridgman growth of semiconductors", *Journal of Crystal Growth*, **263**, pp 80-89 (2004).

24. Ho, C.D., Yeh, H.M. and Yeh, T.L. "Optimal zone lengths in multi-pass zone-refining processes", *Separation Technology*, **6**, pp 227-233 (1996).

25. Ho, C.D., Yeh, H.M. and Yeh, T.L. "Numerical analysis on optimal zone lengths for each pass in multipass zone-refining processes", *The Canadian Journal of Chemical Engineering*, **76**, pp 113-119 (1998).

26. Wang, J.H. and Kim, D.H. "Numerical analysis of melt/solid interface shape in zone melting recrystallization process", *J. Cryst. Growth*, **173**, pp 201-209 (1997).

27. Lan, C.W., Chian, J.H. and Wang, T.Y. "Interface control mechanisms in horizontal zone-melting with slow rotation", *J. Cryst. Growth*, **218**, pp 115-124 (2000).

28. Lan, C.W. and Liang, M.C. "Modeling of dopant segregation in vertical zone-melting crystal growth", *J. Cryst. Growth*, **186**, pp 203-213 (1998).

29. Lan, C.W. and Liang, M.C. "Three-dimensional simulation of vertical zone-melting crystal growth: Symmetry breaking to multiple states", *J. Cryst. Growth*, **208**, pp 327-340 (2000).

30. Lan, C.W. and Liang, M.C. and Chian, C.H. "Supressing three-dimensional unsteady flows in vertical zone-melting by steady ampoule rotation", *J. Cryst. Growth*, **213**, pp 395-407 (2000).

31. Roussopoulos, G.S. and Rubini, P.A. "A thermal analysis of the horizontal zone refining of indium antimonide", *J. Cryst. Growth*, **271**, pp 333-340 (2004).

32. *Fluent 6.1 User's Guide*, Fluent Inc. Lebanon, NH 03766, USA (2003).

33. Boschert, St., Dold, P. and Benz, K.W. "Modeling of the temperature distribution in a three-zone resistance furnace: Influence of furnace configuration and ampoule position", *J. Crystal Growth*, **187**, pp 140-149 (1998).

34. Crochet, M.J., Dupret, F., Ryckmans, Y., Geyling, F.T. and Monberg, E.M. "Numerical simulation of crystal growth in a vertical Bridgman furnace", *J. Crystal Growth*, **97**, pp 173-185 (1989).

35. ASM Handbook, *Properties and Selection: Nonferrous Alloys and Special-Purpose Materials*, **2**, Metals Park, Ohio, American Society for Metals (1983).

36. Yurchak, R.P., Smirnov, B.P. and Kanevskaya, L.S. "Thermal conductivity of solid and liquid tellurium", *Soviet Phys - Semiconductors*, **3**(7), pp 923-925 (1970).

37. Herwig, F. and Hoyer, W. "Viscosity investigations in eutectics", *Solidification and Gravity*, **215**, pp 297-302 (1996).

38. Dost, S., Liu, Y.C., Lent, B. and Redden, R.F. "A numerical simulation study for the effect of applied magnetic field in growth of CdTe single crystals by the travel heater method", *Inter. J. Applied Electromagnetics and Mechanics*, **17**, pp 271-288 (2003).

39. Perez-Geande, I., Rivas, D. and de Pablo, V. "A global thermal analysis of multizone resistance furnaces with specular and diffuse samples", *J. Crystal Growth*, **246**, pp 37-54 (2002).